2

Impact of Nitrogen Ion Density on the Optical and Structural Properties of MBE Grown GaInNAs/GaAs (100) and (111)B Quantum Wells

J. Miguel-Sánchez, Á. Guzmán, A. Hierro, E. Muñoz, U. Jahn, and A. Trampert

The impact of nitrogen ion density, present in the chamber during molecular beam epitaxial growth of the GaInNAs quantum wells, on their structural and optical properties is presented. The growth on two different substrate orientations, GaAs (100) and (111)B has been studied. The quantum well optical emission was found to be strongly increased when the nitrogen ion density was reduced during the growth, as determined by photoluminescence experiments. Cathodoluminescence mappings of quantum wells grown under different ion densities are compared, showing a stronger compositional modulation depth, and thus a higher structural disorder, when a higher ion density is present during the growth. This technique was also used to study the optical activity of defects found in GaAs (111)B samples. We applied deflecting magnetic fields to tune the amount of nitrogen ion density in the chamber during growth. Atomic force microscopy (AFM) measurements in similar epilayers showed that ions cause an important structural disorder of the layers, showing approximately twice the root mean square (RMS) roughness when the density of ions is not reduced by external magnetic fields. Additionally, transmission electron microscopy (TEM) measurements of buried GaInNAs quantum wells is presented, showing that lateral compositional fluctuations of In and N are suppressed when the quantum wells are protected from the ions. Finally, we have found that quantum wells exposed to higher ion densities during the growth show deeper localization levels and higher delocalization temperatures. These results clearly show that the structural properties such as the roughness and the compositional modulation, as well as the optical properties, such as the optical emission and localization energies are strongly dependent on the density of nitrogen ions present in the chamber during the growth of GaInNAs quantum wells. Rapid thermal annealing (RTA) experiments are also consistent with this hypothesis.

2.1 Introduction

2.1.1 Overview

In this chapter, we describe in detail our research concerning the impact of the nitrogen plasma parameters on the optical and structural properties of dilute nitrides. We performed an extensive characterization of this plasma. Optimum parameters for the growth of high quality GaInNAs quantum wells, and a method to decrease the damage produced by such plasma ionic species are presented.

2.1.2 Material Properties, Nitrogen Plasmas, and (111)B

It is known from the literature that the addition of small concentrations of nitrogen to GaInAs layers (typically N mole fractions lower than 5%), cause a strong reduction of the optical quality of quantum wells, due to the formation of nonradiative defects, mainly due to the creation of Ga vacancies [1], interstitial incorporation of nitrogen [2] and damage caused by the ionized nitrogen species from the plasma [3–7]. The formation of the first two types of defects is directly related to the growth dynamics and can be controlled by using the proper growth conditions. In this work, we study the latter type of defects, i.e., those formed by ions generated in the nitrogen plasma, and their impact on the GaInNAs quantum wells (QWs) grown on GaAs (111)B and (100) has been assessed.

In order to incorporate nitrogen in the dilute nitride QW an atomic nitrogen source is needed. The most extended method to achieve this goal in molecular beam epitaxy (MBE) systems is to create a plasma from ultra-pure nitrogen. In these plasmas, different species coexist simultaneously: electrons (e^-), atomic nitrogen (N), diatomic nitrogen (N_2) and their excited species ($N_2{}^+$, etc) [6–8]. The ratio of the ionized species to the atomic species is called ionization factor. The lower this ionization factor, the higher the quality of the plasma for epitaxial growth applications, as we will show in the following sections.

Since electron cyclotron resonance (ECR) plasma sources show high ionization factors [8,9], the most extended nitrogen sources for the growth of nitrides and diluted nitrides are radio frequency (rf) plasmas and direct current (dc) plasmas. In this work, we used an Oxford applied rf source.

To precisely control the amount of atomic nitrogen in the plasma, we used an optical emission detector (OED) that detects the characteristic emission of atomic nitrogen. This device gives an in situ and real-time value proportional to the amount of atomic nitrogen in the plasma. It consists of an optical detector, capped with a narrow band pass optical filter tuned to the emission energy of the photons emitted from excited nitrogen atoms in the plasma.

In the following sections, different ways for in situ characterization of plasmas allowing to determine optimum working conditions for epitaxial growth are described.

In the literature, almost each work devoted to the study of the GaInNAs material refers to the (100) orientation [10–12]. In the present chapter we additionally propose the study of dilute nitride materials grown on the GaAs (111)B substrates. Our motivation is due to the interesting properties of heterostructures grown along this orientation. First of all, the presence of a piezoelectric field in strained heterostructures grown on (111) surfaces of zinc-blende structures [13]. These properties have been extensively studied in the literature for the well-known GaInAs/GaAs (111)B system and an excellent descriptions can be found in [14–17]. With this material system, laser emission up to 1.1 μm has been reached, with low thresholds [18–21]. Additionally, this piezoelectric field has been used for the design of nonlinear devices and optical modulators based on GaInAs/GaAs [22–26]. Recently, the first GaInNAs laser diode grown on GaAs (111)B and working at room temperature was demonstrated by our group [27].

Another interesting property refers to the critical layer thickness on this orientation. Several publications claim that the theoretical critical layer thickness is greater than for GaAs (100) [28, 29]. However, some experimental results seem to indicate that the critical layer thickness is approximately the same [30, 31].

Apart from above features, an additional interesting property of the GaAs (111)B surface is the difficulty to find a transition from the 2D to the 3D Stranski–Krastanov growth mode. There is some controversy in the literature about this point, since some authors could not find any 3D growth mode [31–33], but on the other hand, some authors reported the growth of quantum dots on GaAs (111)B [34–39]. This problem could be interesting for the growth of dilute nitrides to avoid the transition to 3D growth mode reported in the literature for GaInNAs on GaAs (100), under certain growth conditions. Additionally, if the critical layer thickness is higher, higher In mole fraction could be incorporated in the QWs without relaxation, so longer wavelengths with high-optical quality material could be achieved.

2.2 Experimental Setup

Samples characterized in this chapter were grown by MBE in a Riber 32 machine equipped with a rf plasma source. The structure of the GaAs (111)B samples is a p–i–n diode, unless otherwise stated in the text. It consists of a 500 nm intrinsic region between 300-nm thick p^+ and n^+ regions doped with beryllium and silicon, respectively. In the middle of the intrinsic region, a 7-nm thick GaInNAs quantum well was grown.

Photoluminescence (PL) characterization was performed using a He–Ne laser, with samples cooled in a cryogenic system down to 16 K. Light was collected and focused by two lenses, dispersed by a computer-controlled monochromator, and finally detected by a cooled Ge detector.

RTA were performed in a conventional RTA oven under a 1.3 bar nitrogen pressure with samples sandwiched between two dummy GaAs pieces.

2.3 Plasma Characterization

2.3.1 Basic Characterization

To achieve an accurate control of the plasma properties we can tune two different external parameters: the molecular nitrogen flux and the applied rf power. In this section, we will show techniques, which are suitable to characterize nitrogen plasmas in an effective manner. So, plasma conditions can be achieved allowing for the fabrication of GaInNAs QWs with optimum optical emission properties.

The basic plasma characterization is to determine the amount of atomic nitrogen found in the plasma cavity for each applied power and nitrogen flux. For that purpose, we measured the OED intensity as a function of the applied power, for several nitrogen fluxes. Additionally, this basic measurement is valid to perform a calibration of the system, in order to know the amount of nitrogen for each pair of rf power and nitrogen flux. The OED characterization of the plasma used in this work is shown in Fig. 2.1 for three different nitrogen fluxes: 0.3, 0.5, and 1.0 standard cubic centimeter per minute (sccm).

For low rf powers (lower than 70 W), no stable plasma could be ignited in our system, which is the reason for the absence of data points for that range of powers in the curves shown in Fig. 2.1. By increasing the applied power, the OED output increases. For powers between 70 and 200 W the difference for the three nitrogen fluxes is almost negligible. This difference increases as the applied rf power is increased, specifically for rf powers higher than 200 W, approximately. Thus, at the highest applied powers, there is an increment of

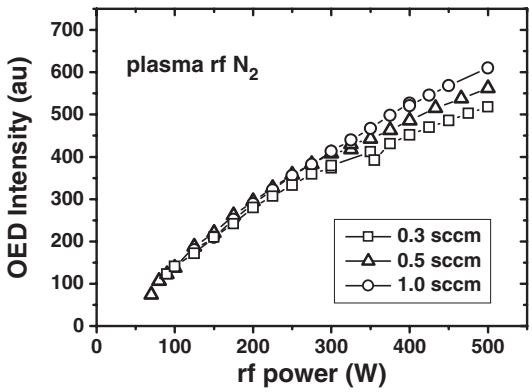

Fig. 2.1. OED characterization as a function of the applied rf power for three different nitrogen fluxes

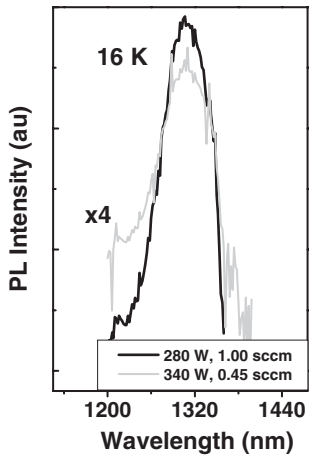

Fig. 2.2. Low-temperature (16 K) PL spectra of two GaInNAs QWs, grown under the same conditions, except for plasma parameters: 280 W and 1 sccm (*black line*) as well as 340 W and 0.45 sccm (*grey line*). OED intensity was the same for both samples

active nitrogen (OED) of up to 20% when the nitrogen flux is increased from 0.3 to 1.0 sccm.

To effectively verify that the OED signal is strongly correlated to the nitrogen content incorporated in the dilute nitride samples, the following experiment was performed: Two p–i–n structure samples were grown on GaAs (111)B (exhibiting the previously described structure), using exactly the same growth conditions for both samples (substrate temperature, growth rate, As flux, and OED intensity). The only difference between both samples was the plasma conditions to achieve the same OED intensity. We used two different powers, 280 and 340 W applied to two different nitrogen fluxes of 1.00 and 0.45 sccm, respectively, to achieve exactly the same OED value. In Fig. 2.2, low-temperature PL spectra of both samples are shown.

Both spectra are vertically shifted for clarity. The PL peak emission from both samples is exactly at the same wavelength (within measurement errors). As the In contents from both samples are nominally the same, we can finally conclude that the OED output is a reliable parameter for the accurate control of the nitrogen mole fraction in GaInNAs QWs grown by MBE. Additionally, in this figure, it is shown that the emission from the sample grown with the lower rf power (280 W) is stronger than the emission from the sample grown with the higher rf power (340 W). Thus, we may conclude that it is the rf power and not the flux that determines the optical quality of GaInNAs QWs. A lower structural quality of samples grown with higher nitrogen fluxes is expected, since high nitrogen fluxes strongly decreases the mean free paths of atoms and molecules in the chamber and over the surface. For this reason, further experimental parameters, apart from rf power and nitrogen flux, must

be taken into account to control the optical quality of GaInNAs QWs, as it will be shown in following sections.

2.3.2 The Modified Langmuir Probe Method

In order to characterize rf plasmas, electrical methods were commonly used in the past. The most spread one is based on Langmuir and consists of a narrow metallic wire (probe) introduced in an ignited plasma. By biasing this wire, current–voltage measurements were obtained, from which important plasma parameters can be extracted to characterize the plasma [8]. For dilute nitrides growth, the plasma characterization found in the literature was almost exclusively optical [6,7,40]. By a careful inspection of the optical emission coming from the plasma, radiative transitions of various species (atomic, excited, molecular, etc.) could be detected and measured in the plasma. This method is very accurate, but requires the presence of complex optical equipment near the plasma source, which is sometimes not possible due to the position of the cells in the growth chambers. Additionally, the characterization of the plasma performed in this way gives information about the plasma inside the nitrogen source, in which completely different conditions may hold when compared to the plasma impinging onto the sample.

In this section we present an easy and novel electric method for in situ plasma characterization at the sample position, where the conditions must be accurately known to control the epitaxial growth process, since it is in this region where growth dynamics and thermodynamics determine the characteristics of the grown material [41].

This novel method is based on the use of a Bayard–Alpert vacuum gauge as a modified Langmuir probe. Bayard–Alpert gauges are found in almost every ultra-high vacuum system (UHV system) and in MBE systems, due to the need of accurate pressure measurements in the 1×10^{-5} to 1×10^{-11} Torr range. The operation of these gauges is as follows: a tungsten filament is heated producing electrons due to the thermionic effect. A biased grid accelerates these electrons. When these electrons travel through an effective cross section of the atomic or molecular species in the vacuum, ionization occurs by the lost of an electron from the outer shells of these gaseous species. Finally, ionized species impinge onto a narrow metallic wire (collector), being collected and generating an electric current directly proportional to the amount of particles in the chamber that is proportional to the pressure at every moment. In standard MBE chambers, this gauge can be moved to exactly the same position of the growing surface. This allows the precise characterization of the incident flux that combined with precise reflection high electron energy diffraction (RHEED) observations permit an accurate calibration of the growth rate for several material systems [41].

On the other hand, the Langmuir probe consists of a short metallic wire introduced in the plasma cavity. Charged species impinge onto the probe

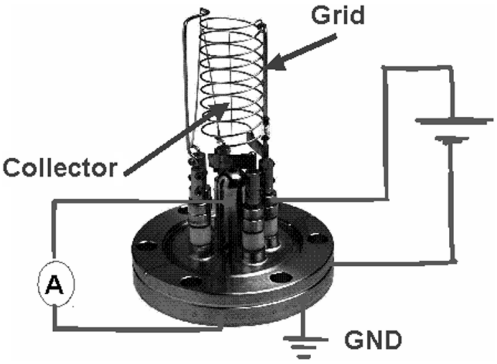

Fig. 2.3. Schematic view of the biasing of a Bayard–Alpert gauge to be used as a modified Langmuir probe

generating a current in an external circuit proportional to their density. Typically, these probes are biased to obtain I–V characterization of the plasma, as stated above [8]. The proposed method takes the advantages from both the gauge and the probe: the plasma has to be characterized at the sample position, to obtain an accurate measurement of the ions impinging onto it during growth. For this purpose, we propose a vacuum-gauge triode-like configuration for the Bayard–Alpert gauge to work as a modified Langmuir probe (Fig. 2.3), with the plasma acting as a cathode. A precision electrometer is connected in series with the probe collector. This will work as the anode. Thus, the different charged species impinging onto it will generate a positive or negative current, depending on the charge of the incident particles. The grid of the probe will act as the deflection grid found in electronic vacuum valves. A voltage source is connected in series with the grid to bias it. Thus, if the bias voltage is negative, negatively charged species from the plasma will be deflected, and therefore a positive current will be measured. In the literature, this is called ion saturation region. On the other hand, when a positive bias is applied to the grid, positively charged species (ionized atoms and molecules) will be deflected, which will yield a negative current, the electron saturation region. Thus, by using this technique we could directly measure the I–V characteristics of the generated plasma in our system, as shown in Fig. 2.4.

Using this setup, the typical characteristics expected from a conventional Langmuir probe are obtained [8]. In our system, by applying bias voltages lower than $-60\,\mathrm{V}$, a positive current is obtained in the ion saturation region. As reducing the bias voltage, the measured current turns negative due to the reduction of the electron shielding: the amount of electrons deflected is reduced. For bias voltages higher than $50\,\mathrm{V}$, the I–V characteristics show another plateau, the electron saturation region, where ions are deflected and electrons attracted toward the collector. With the proposed model, we have

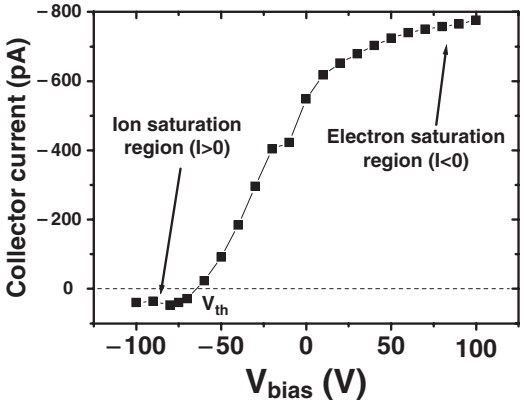

Fig. 2.4. Typical I–V characteristics of our nitrogen plasma, obtained with the modified Langmuir probe. In the figure, ion and electron saturation regions are shown

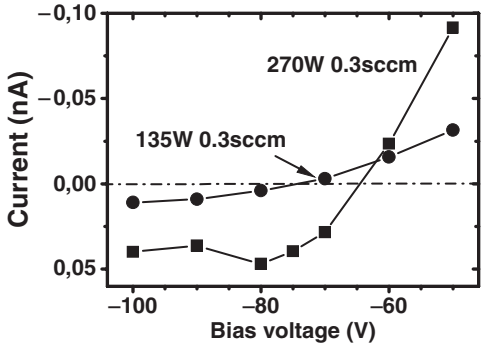

Fig. 2.5. Detail from the ion saturation region of the I–V characteristics from two plasmas generated using the same nitrogen flux (0.3 sccm) and two different rf powers, 135 W (*circles*) and 270 W (*squares*)

detected a positive current generated in the probe that could be only due to positively charged species impinging onto the collector. Thus, we have measured a nonnegligible amount of ionic nitrogen species coming from the plasma during the growth of dilute nitrides.

To assess this point, we performed the I–V plasma characterization for the same nitrogen flux, but using two different applied rf powers, 135 and 270 W (giving rise to different OED intensities, 195 and 356 a.u.). A detail of the ion saturation region from the measured I–V characteristics is shown in Fig. 2.5. According to this data, the application of higher rf powers to the same nitrogen flux yields a more positive current. Thus, we can conclude that the positively charged species measured using this novel modified Langmuir probe method originate from the ignited plasma and are not due to the self-ionization of

the gas due to the grid biasing (these biases are still much lower than the usual bias voltage applied to typical Bayard–Alpert gauges, around 150 V). The objective of the modified Langmuir probe method is the detection and the quantification of ions arriving at the position of the sample. To use this method for an exact quantization of the ion density (charged particles per unit surface in a time unit), impinging onto the surface, a detailed theoretic treatment, a more accurate knowledge of the geometry of the system, and an exact measurement of the area of the collector are needed. On the other hand, this method can be readily used for the optimization of the plasma parameters, to minimize the generated amount of ions, for a given amount of active nitrogen. This is the main objective, since, as previously stated, ionic nitrogen species strongly damage the optical properties of the grown materials [3–5, 42]. To choose the optimum conditions, a set of measurements have been performed, as described below. The first experiment consists of the measurement of the collector current (directly correlated with the amount of ions found in the chamber) for different applied rf powers for three different nitrogen fluxes. The results of these measurements are depicted in Fig. 2.6.

For a given rf power typically used in the growth experiments (below 350 W, in our system), we observe that the lower the nitrogen flux, the lower the measured collector current. If we now measure the amount of nitrogen atoms by reading the OED intensity for several fluxes (Fig. 2.7), it is also observed that the lower the nitrogen flux the lower the OED intensity, for a given applied rf power. This variation is almost negligible (around 3% for a given OED intensity). We can thus conclude that for a given amount of nitrogen to be incorporated in the samples (a given OED, for given growth conditions) the amount of ions is minimized by using a lower nitrogen flux. This nitrogen flux cannot be reduced indefinitely, since there is a minimum flux, for which ignited plasma turns unstable and eventually disappears. Other groups [43] have drawn the same conclusions using other techniques.

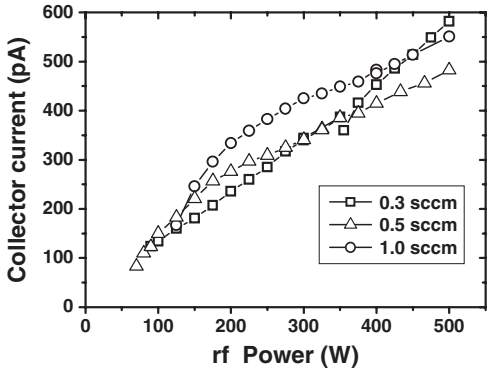

Fig. 2.6. Collector current measured by the modified Langmuir probe as a function of the applied rf power, for three different nitrogen fluxes, 0.3 (*squares*), 0.5 (*triangles*), and 1.0 sccm (*circles*)

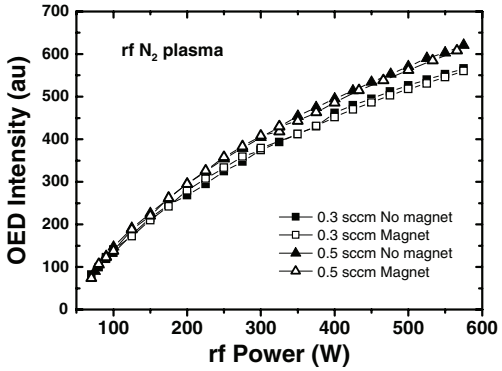

Fig. 2.7. OED intensity as a function of applied rf power for two different nitrogen fluxes, 0.3 sccm (*squares*) and 0.5 sccm (*triangles*), with and without the application of a magnetic field (*filled and hollow symbols*, respectively)

2.3.3 Application of Magnetic Fields to Nitrogen Plasmas

Previously, basic measurements allowed us to easily find the optimum conditions to minimize the amount of ions in the MBE chamber during the growth of dilute nitrides. As we are dealing with ions, we must note that these charged species can interact with electromagnetic fields. Other authors proposed in the past the application of electromagnetic fields to deflect ions generated in DC [3] and ECR [44] plasmas. In our case, we will use static magnetic fields to deflect the ionic species. With the measurement setup proposed in Sect. 2.2, we will check the effect on the QWs of the ion deflection by the magnetic field.

The first step is to check the effect of the magnetic field in the normal operation of the plasma source. In practice, to apply this static magnetic field, a 0.2 T magnet was used, placed under an extension tube between the plasma source and the growth chamber. In this position, the magnetic field lines are perpendicular to the flux of nitrogen species from the source to the sample. The position was chosen by minimizing the current measured by the modified Langmuir probe. The OED intensity, for two different nitrogen fluxes, and the effect of the application of a magnetic field are shown in Fig. 2.7. For comparison purposes, measurements carried out with no magnetic field are also shown in Fig. 2.7. We can observe that the OED intensity obtained by applying the magnetic field is slightly higher than the OED intensity when no field is present. This effect could be due to an enhancement of the confinement of the plasma due to the magnetic field. On the other hand, this difference is almost negligible for the applications used in this work, lower than 2% and comparable to the 1% resolution of our OED measurement system. Thus, we can conclude that the operation of the nitrogen source is not significantly altered by the presence of the magnetic field.

We can now use the modified Langmuir probe to check the effect of the magnetic field on the ions (Fig. 2.8). It is clear from this figure that the

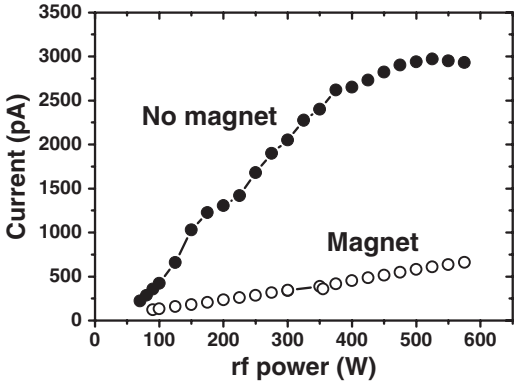

Fig. 2.8. Measured current by the modified Langmuir probe as a function of the applied power (W), for a given nitrogen flux (1 sccm). *Hollow* and *filled symbols* represent the date with and without the application of the magnetic field

application of a magnetic field reduces the collected current, and thus, it reduces the amount of ions reaching the sample. In the following sections we will show how the ion density present during the growth, impinging onto the sample, strongly affects the optical and structural properties of the GaInNAs quantum wells grown on GaAs (111)B and (100), and how the reduction of this density by the application of magnetic fields strongly reduces the damage introduced in the quantum wells during growth.

2.4 Minimizing the Impact of the Ions

In this section we will briefly describe how the ratio of the incorporated nitrogen atoms and the density of ions in the chamber can be tuned. Using these techniques, different samples with different [N]/[N_{ion}] ratio can be grown [42], to check whether the reduction of the ions effectively enhances or not the optical sample quality.

The nitrogen concentration [N] incorporated to the samples was deduced from QW photoluminescence measurements. Additionally, [N_{ion}] is proportional to the collected current using the modified Langmuir probe, as stated in previous sections. Thus, as we are dealing with a plasma, two approaches can be used to modify the [N]/[N_{ion}] ratio: using the nitrogen cell shutter and by the application of a magnetic field. By the combination of the two techniques, we grew three equivalent samples, on GaAs (100), using the same growth conditions, with the only difference in the [N]/[N_{ion}] ratio, as described below and in Fig. 2.9.

The three samples were 7-nm thick single GaInNAs single QWs, with a 100 nm GaAs cap and barrier layer. A first sample was grown (sample A, Fig. 2.9a), under the application of a magnetic field in the way explained in

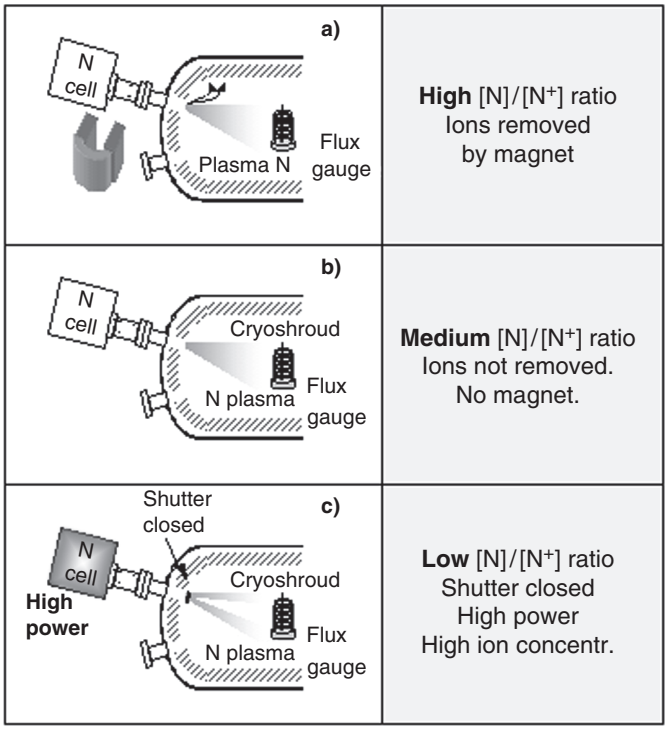

Fig. 2.9. Schematic diagram of the growth procedures for samples A, B, and C, described in the text, with low, medium, and high ion concentrations during the growth, respectively

Sect. 2.3.3. The following sample was grown exactly under the same conditions, using no magnetic field deflection (sample B, Fig. 2.9b). The third sample was grown with the nitrogen cell shutter closed (sample C, Fig. 2.9c). In order to achieve a similar N incorporation in the sample a higher rf power was applied, since the shutter does not interrupt but strongly reduces the flow of atomic and ionic species toward the sample.

Due to this high power, the current measured by the modified Langmuir probe, when the cell shutter was closed, was still very high. For this reason, sample C has the lowest $[N]/[N_{ion}]$ ratio of the three samples. Sample A has the highest ratio, since exactly the same N contents are found for this and for sample B, but the ion density was strongly reduced by the magnetic deflection. For the three samples, low-temperature photoluminescence measurements were carried out to compare their optical properties. The results are shown in Fig. 2.10.

In Fig. 2.10a, the low-temperature (16 K) PL peak intensity is shown as a function of the $[N]/[N_{ion}]$ ratio. As seen in this figure, the higher this ratio, the higher the PL intensity, which implies a lower concentration of

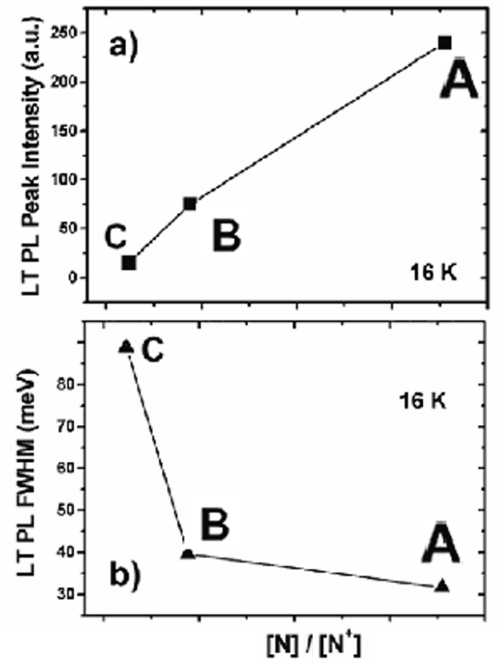

Fig. 2.10. PL peak intensity (**a**) and FWHM (**b**) of the A, B, and C samples described in the text, for several ion contents

nonradiative recombination centers. Full width at half maximum (FWHM) from the same measurements is shown in Fig. 2.10b. There we can clearly observe that this FWHM is wider (lower optical quality) when the $[N]/[N_{ion}]$ decreases. From these experiments we can conclude that the utilization of higher powers combined with a closed cell shutter is not a reliable procedure for the development of good quality dilute nitride-based optoelectronic devices. For this reason, this method was not employed in this work. We will focus on the growth of quantum wells with and without the application of magnetic fields, thus varying the $[N]/[N_{ion}]$ ratio, and studying the effect of these ions on the optical and structural properties of dilute nitride quantum wells in the following sections.

2.5 The Role of Ions on GaInNAs/GaAs (111)B QWs

To study the impact of these ionic species on the optical properties of GaInNAs/GaAs (111)B QWs two equivalent samples were grown, with the only difference that the first of the samples (IM1) was grown under the application of a magnetic field, and the second sample (NIM1) was grown conventionally. The structure of both samples is the p–i–n diode described in previous sections. There is an evident difference between the photoluminescence

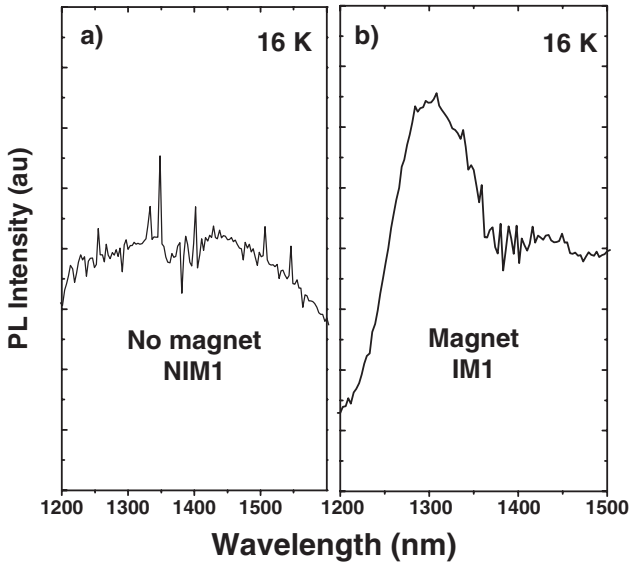

Fig. 2.11. (**a**) PL spectrum (16 K) of the NIM1 sample, grown with no magnet. (**b**) Low-temperature (16 K) PL spectrum of the IM1 sample, grown with the magnetic deflection

spectra from both samples. In Fig. 2.11 the low-temperature (16 K) photoluminescence spectra of both samples are shown. We can observe how the IM1 sample shows a well-defined peak at 1,300 nm, with the usual energy tail related to the formation of low energy states below the band gap. On the other hand, the sample grown without the magnet, and thus with a higher ion density present in the chamber during growth, shows no clear peak emission, but a very broad emission. The impact of the ions on the optical properties of GaInNAs is thus shown: higher ion densities degrade the optical properties of the QWs like in the case of GaAs (100) (see Sect. 2.4).

As widely reported, a RTA cycle maximizes the optical emission of QWs [3, 11, 12, 15]. We describe now some results regarding the behavior of both samples IM1 and NIM1 after different RTA cycles. In Fig. 2.12, we show how after RTA annealing (30 s at 850°C) both samples show a well-defined peak.

The cycle used in this experiment was chosen based on results of our previous experiments. For each sample (growth conditions) this optimum cycle has to be studied, since it strongly depends on the structural quality of the as-grown material [45]: The lower the structural quality of the GaInNAs quantum wells (compositional modulation, undulation of the interfaces), the higher the optimum RTA temperature, for a given dwell time. For these reasons, we performed a detailed RTA characterization of samples IM1 and NIM1, to extract indirectly structural information from the QWs. The results of such experiments are shown in Fig. 2.13.

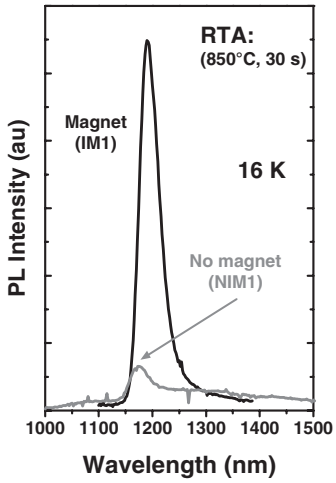

Fig. 2.12. Low temperature, 16 K, PL spectrum of the sample NIM1 (*grey line*) and IM1 (*black line*), after a RTA process (30 s at 850°C)

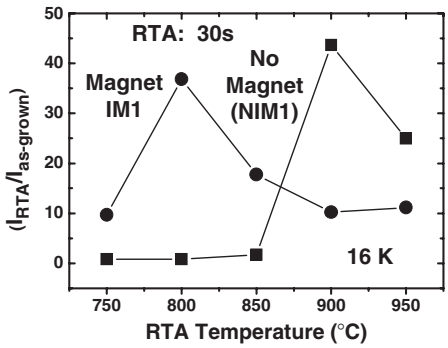

Fig. 2.13. Relative increment of the PL intensity after RTA annealing, for a dwell time of 30 s. No magnet: *squares*, magnet: *circles*

There we have plotted the relative increase of the measured intensity after annealing when compared to its as-grown value. 30 s was the annealing time for all the experiments. We can clearly observe that the optimum annealing temperature is much lower for the IM1 sample than for NIM1 sample, what is consistent with a higher structural quality of the GaInNAs quantum well sample grown under the lower density of ions.

Another effect produced by the RTA annealing is the shift of the quantum well emission toward higher energies (blueshift). If we compare this shift from both samples, as a function of the annealing temperature (Fig. 2.14), we observe a strong difference in blueshifts from both samples assuming that IM1 and NIM1 samples contain the same nominal N mole fraction: In that case, for the sample IM1 the blueshift would be much lower than for sample NIM1. We

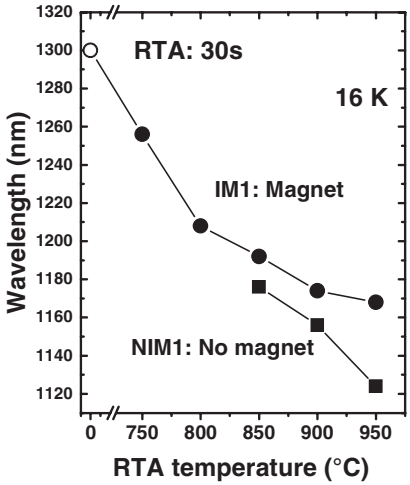

Fig. 2.14. Peak wavelength of the low-temperature PL spectra after RTA annealing, for a dwell time of 30 s. No magnet: *squares*, magnet: *circles*

will see in the following section that this reduced blueshift using ion deflection is confirmed in the case of GaInNAs/GaAs (100) QWs. In this figure, the absence of data for the as-grown sample and for the lower temperature annealing is due to the fact that no clear peak emission could be measured from this sample. This is an important result, since we have determined a method to reduce blueshifts in dilute nitride samples for given nitrogen contents. Thus, to achieve a given wavelength in the design of the optoelectronic device, a slightly lower nitrogen contents have to be incorporated into the quantum wells when using the magnetic deflection. This effect will give rise to an enhanced emission from the QW, since it is known in the literature that an increase in nitrogen content in the GaInNAs QWs yields to a reduction in their optical quality. As shown in Sect. 2.6, similar results are found for the GaInNAs/GaAs (100) system. Therefore, we can tentatively conclude that the reduction of nitrogen ions during the growth enhances the formation of In–N bonds, more favorable energetically [46], what would explain the reduced blueshift and the stronger emission from these samples [47, 48].

2.6 The Role of Ions on GaInNAs/GaAs (100) QWs

The observations and measurements found in Sect. 2.5 for the GaInNAs on GaAs (111)B quantum wells are not exclusive for this material system. In this section we will describe the impact of the ions on the optical and structural quality of GaInNAs quantum wells grown on GaAs (100).

2.6.1 Optical Characterization

For this purpose, we studied the optical properties of two equivalent samples, consisting of 7-nm thick GaInNAs QWs (nominal In and N mole fractions of 30% and 1.7%, respectively). A 100-nm thick GaAs barrier and cap layer was grown over both QWs. As described in the previous section, the only difference between both samples is again the application of magnetic fields during the growth of one of the samples (IM2), whereas the second sample (NIM2) was grown conventionally, with no ion deflection. Thus, to achieve a given wavelength in the design of the optoelectronic device, a slightly lower nitrogen contents have to be incorporated into the quantum wells when using the magnetic deflection. This effect will give rise to an enhanced emission from the QW, since it is known in the literature that an increase in nitrogen content in the GaInNAs QWs yields to a reduction in their optical quality. As shown in the following section, similar results are found for the GaInNAs/GaAs (100) system. Therefore, we can tentatively conclude that the reduction of nitrogen ions during the growth enhances the formation of In–N bonds, more favorable energetically [46], what would explain the reduced blueshift and the stronger emission from these samples [47, 48].

Photoluminescence Measurements

Low-temperature PL measurements are shown in Fig. 2.15. As seen in this figure, and as it was found for GaInNAs on GaAs (111)B, sample IM2, grown with the lower ion density, shows a stronger luminescence (four times higher) and a 10 meV narrower FWHM. This comparison was performed at room

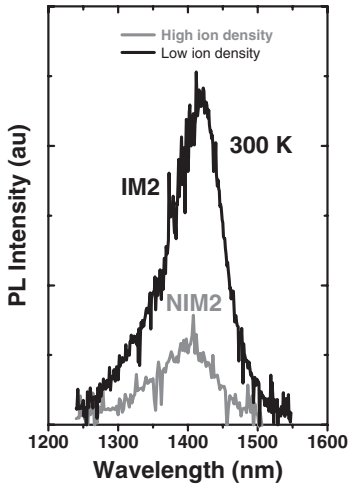

Fig. 2.15. Room Temperature PL measurements of the IM2 (*black line*) and NIM2 (*grey line*)

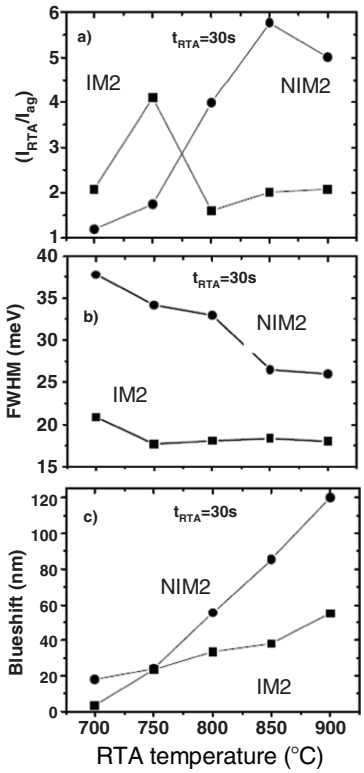

Fig. 2.16. PL (16 K) experiments for different annealings of the IM2 and NIM2 samples (*squares* and *circles*, respectively) (**a**) Increment of the PL intensity relative to the as-grown intensity. (**b**) FWHM. (**c**) Blueshift after annealing. The annealing time was 30 s in all the cycles

temperature, where localization effects are almost negligible for these two samples. The impact of the ion nitrogen density on the optimum annealing temperature was also measured for these samples, similarly to what we did for the (111)B orientation. In Fig. 2.16a, we show the ratio of the peak intensity after annealing to the as-grown intensity. We clearly observe that the optimum temperature for the sample grown without the magnet is much higher than for the sample IM2. Thus, to achieve a given wavelength in the design of the optoelectronic device, a slightly lower nitrogen contents have to be incorporated into the quantum wells when using the magnetic deflection. This effect will give rise to an enhanced emission from the QW, since it is known in the literature that an increase in nitrogen content in the GaInNAs QWs yields to a reduction in their optical quality. As shown in the following section, similar results are found for the GaInNAs/GaAs (100) system. Therefore, we can tentatively conclude that the reduction of nitrogen ions during the growth enhances the formation of In–N bonds, more favourable

energetically [46], what would explain the reduced blueshift and the stronger emission from these samples [47, 48].

If we measure the blueshift of the PL emission, we observe how for annealing temperatures greater than 750°C this blueshift is lower for the samples grown under a lower ion density. This is again a positive result for the development of optoelectronic devices based on dilute nitrides: the application of magnetic fields implies that a lower blueshift will appear after annealing. Thus, in the design of the GaInNAs QW-based optoelectronic devices lower nitrogen mole fraction should be incorporated in the growth process to achieve a given final (after annealing) emission wavelength of the device. The introduced procedure yields to a double enhancement of the emission of the QWs: ion deflection reduces nonradiative centers and the lower nitrogen content to be incorporated additionally improves optical quality.

Cathodoluminescence Measurements

Although cathodoluminescence (CL) at these wavelengths is a powerful tool for the analysis of GaInNAs material, only very few reports have been published about this topic [12, 49]. We obtained CL mappings at 10 K. Some results are shown in Fig. 2.17.

The darker area shown in the sample grown with no magnetic field, NIM2 (Fig. 2.17a), is caused by a dust particle on the surface, as observed in the corresponding SEM image (not shown). Both figures show a rather homogeneous lateral distribution of the luminescence intensity, but a slight granularity is detected in both images. To analyze this CL distribution quantitatively, we performed CL intensity profiles or line scans.

Results of such measurements are shown in Fig. 2.18 performed at the same energy as the CL mappings of Fig. 2.17. The intensity fluctuations visible in this figure show areas of different brightness of around 4 μm in diameter. These were previously observed in GaInNAs material by Kitatani et al. [12], who reported similar granularity in the same scale. To directly compare both

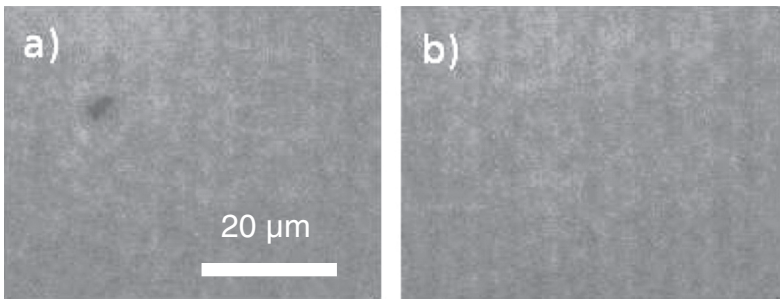

Fig. 2.17. (×2,000) CL images of (**a**) NIM2 sample (no magnet) at 1,330 nm and (**b**) IM2 sample (magnet) at 1,300 nm. Scale is indicated by the *white line*

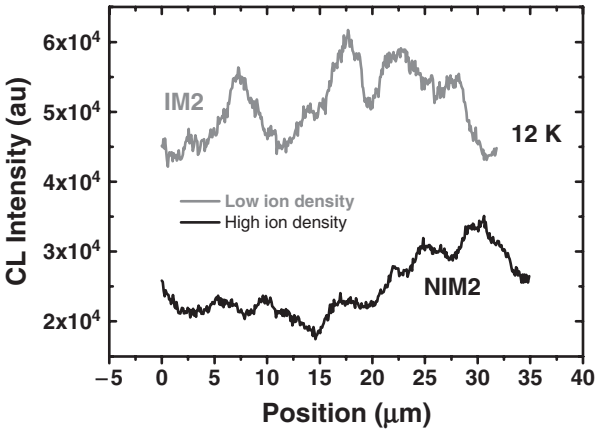

Fig. 2.18. CL emission from samples IM2 and NIM2, (*grey* and *dark lines*, respectively), at 12 K

line scans, we used the RMS modulation depth, as defined in [50]. We can then directly compare both samples. Calculations of this parameter yield values of 17.3% and 9.7% for samples NIM2 and IM2, respectively. The modulation depth reveals the underlying disorder of the GaInNAs QW [50, 51] and indicates a higher degree of disorder for the sample grown without magnetic field. This conclusion is consistent with the previous experiments (RTA annealing and photoluminescence). In Sect. 2.6.2 we will describe structural measurements that corroborate our hypothesis of a better quality of the GaInNAs QWs grown under an applied magnetic field.

2.6.2 Structural Characterization

To complement the optical measurements presented in Sect. 2.6.1, we performed some structural analysis, using two different microscopy techniques, AFM and TEM.

Atomic Force Microscopy

To use this powerful characterization tool for the analysis of GaInNAs material, we grew two equivalent 7-nm thick epilayers, with the same composition than NIM2 and IM2 QWs, and which we will call NIM3 and IM3, for the conventionally grown epilayer and under the application of a magnetic field, respectively. These epilayers were grown under exactly the same conditions of IM2 and NIM2 QWs. Plasma and nitrogen flux were immediately stopped after the completion of the epilayer.

Figure 2.19a, b show two 500 × 500 nm regions for both samples. Figure 2.19c, d show the same region with a higher detail (180 × 180 nm).

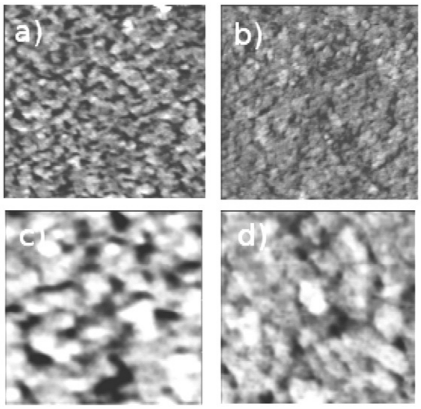

Fig. 2.19. Atomic force microscope scans of samples NIM3 (no magnet, figures a and c) and IM3 (magnet, figures b and d). Scan scales: (**a**) 500 × 500 nm. (**b**) 500 × 500 nm. (**c**) 180 × 180 nm. (**d**) 180 × 180 nm

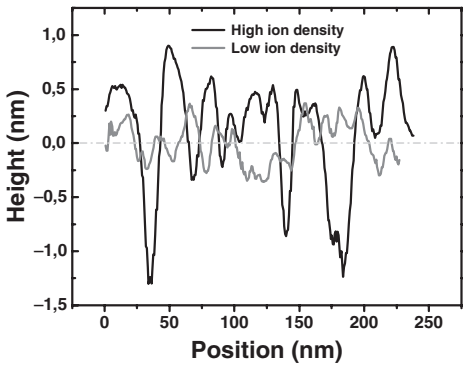

Fig. 2.20. Height profiles from the surfaces shown in Figs. 2.19a, b. *Grey* and *black lines* represent the section profiles of IM3 (magnet) and NIM3 (no magnet) samples, respectively

In Fig. 2.19a the NIM3 epilayer is shown, grown under the usual ion density in the chamber. This image shows a great modulation of the surface, and the presence of holes tens of nanometers wide. The formation of such holes has been observed by other groups previously [52].

The depth of some holes is higher than ten atomic monolayers. In the scanned area the RMS roughness of this surface is 0.53 nm. Figure 2.20 shows profiles of a random section from both surfaces. In these profiles, the fluctuations of the surface can be easily observed. Undulations of the same magnitude have been observed for GaInNAs QWs by other groups [53].

On the other hand, if we observe the IM3 surface (Fig. 2.19b), grown with a lower ion density, we can clearly see a flatter, more homogeneous, and compact

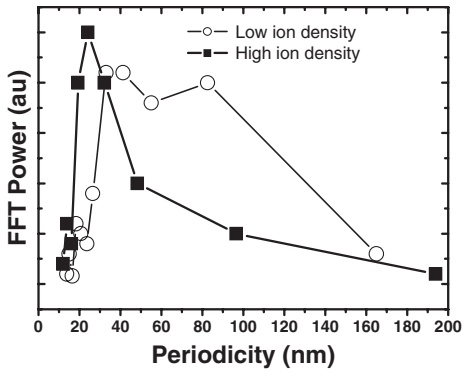

Fig. 2.21. Normalized fast Fourier transform of a mean section (shown in Fig. 2.20) of the surfaces from samples IM3 (magnet) and NIM3 (no magnet), represented by *white circles* and *dark squares*, respectively

layer, with a RMS roughness of only 0.35 nm, almost half that of NIM2. The profile measurements show that only fluctuations from one to four monolayers are found. Thus, we can conclude from these measurements that the application of the magnetic fields strongly reduces the roughness of the upper layer from GaInNAs QWs, for given growth conditions. The statistical analyses of every section of the images give rise to similar results. In Fig. 2.21 we show the mean fast Fourier transform (FFT) taken from several profiles from the surfaces. We obtain from this transform information about the periodicity of the features of the surfaces. Continuous lines are interpolations between the points, representing the data. As seen in this figure, we observe a clear periodicity in patterns (holes) in the sample grown with no magnetic deflection (black squares), with strong components with periods between 20 and 50 nm. On the other hand, if we repeat the analysis for sample IM3, we obtain different results: a wide band (white circles) is obtained, which indicates a more flat surface, with no apparent periodicity due to surface modulation.

Transmission Electron Microscopy

Structural properties of GaInNAs material are quite sensitive to the growth parameters [54] and to the growth temperature in particular [55]. This growth temperature must be low (compared to the optimum growth temperatures for materials such as GaInAs, around 450°C), to suppress 3D or Stranski–Krastanov growth mode and minimize the formation of undulations from the upper quantum well interface. Additionally, an intermediate step between 2D and 3D modes was described in the literature, consisting of the 2D growth mode, with the formation of a lateral composition modulation from In and N mole fractions, with modulations periods in the range of 10–50 nm, typically [56–58]. These modulation fluctuations are directly related to the incorporation of N, since these variations have not been found such strongly in GaInAs

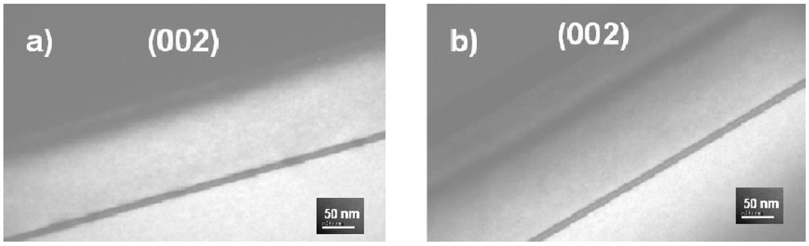

Fig. 2.22. TEM micrographs ($g = 002$) from NIM2 (**a**) and IM2 (**b**). The growth direction was from the *bottom* to the *top* of the figures

QWs, and as shown in [53]. In this section we show how this lateral composition modulation is strongly reduced if the ion density in the growth chamber is reduced. For this reason, we studied samples IM2 and NIM2 by TEM.

Figure 2.22a, b show TEM photographs taken with a diffraction vector $g = 002$, sensible to the material composition [53, 56]. As observed in this figure, we only see slight fluctuations in the upper interface of the QW, indicating that no 3D growth mode occurred. This is consistent with the streaky patterns observed in the RHEED during the growth. A slight modulation of the upper interface is observed for sample NIM2 (Fig. 2.22a). In addition to this fluctuation, a lateral composition modulation is also observed. This fluctuation is caused by the simultaneous incorporation of In and N, as shown in [56]. This modulation has not been observed for InGaAs. These composition fluctuations are spaced apart between 20 and 100 nm, as depicted in Fig. 2.22a. The period of this fluctuation is in the same range than that found in the previously showed AFM measurements. Analyzing sample IM2, shown in Fig. 2.22b, we cannot now appreciate fluctuations in QW thickness, which is consistent with a perfect 2D growth mode. Additionally, no compositional modulation was found along the QW. With this experiment, we have a direct evidence of the strong correlation of the ion density present in the chamber during the growth and the lateral composition modulation of the GaInNAs QWs: When this density is reduced by the application of magnetic fields this lateral composition modulation is suppressed for QWs grown under exactly the same conditions.

Figure 2.23 shows a high-resolution TEM micrograph from sample IM2. Here we can appreciate the high quality of the quantum well and its interfaces. Upper and lower interfaces are almost undistinguishable. Only variations of very few monolayers are to be seen in the micrograph.

Effect of Plasma Ions on Carrier Localization

The incorporation of small nitrogen quantities in GaInNAs QWs shifts the gap of the material toward lower energies [10]. But additionally, a nonnegligible density of localized states is formed below the GaInNAs conduction band

Fig. 2.23. High-resolution TEM micrograph of IM2 sample, grown with the low-ion density

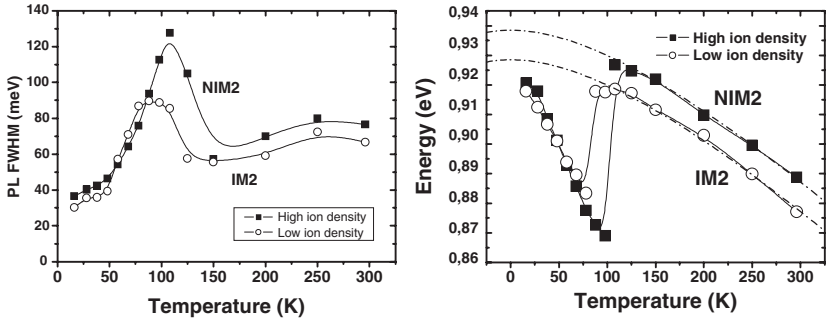

Fig. 2.24. *Left*: PL peak energy as a function of the temperature for samples IM2 and NIM2, *white circles* and *black squares*, respectively. The *continuous lines* are β-spline interpolations between the data. *Dashed-dotted lines* are Varshni fits to the data. *Right*: evolution of the FWHM of the PL spectra as a function for the temperature for the same samples IM2 and NIM2

[56]. Several experiments have been made to detect and characterize them. In photoluminescence at different temperatures we can observe S-shape behavior of the QW peak emission [59,60]. PL spectra from IM2 and NIM2 QWs, similar results are shown in Fig. 2.24.

The peak energy emission from both samples is plotted in this figure by white circles and black squares, for samples IM2 and NIM2, respectively. Solid lines are β-spline interpolations between experimental data, drawn as a guide for the eye. Dashed-dotted lines are fittings to the Varshni model, which describes the variation of the gap with temperature. These fittings were also performed by other authors for GaInNAs QWs with good results [60]. Varshni's formula, to be fitted, is

$$E(T) = E(0) - \frac{\alpha T^2}{T + \beta}. \tag{2.1}$$

Table 2.1. Parameters used in Varshni fits for the single quantum well GaInNAs samples IM2 and NIM2, shown in Fig. 2.24

Parameter	IM2	NIM2
α	3.4×10^{-4} eV K^{-1}	3.4×10^{-4} eV K^{-1}
B	296 K	296 K
$E(0)$	0.9285 eV	0.9385 eV

Table 2.2. Localization parameters measured for the single quantum well GaInNAs samples IM2 and NIM2, shown in Fig. 2.24

Parameter	IM2	NIM2
T_{loc}	77 K	100 K
E_{loc} (16 K)	10 meV	18 meV
E_{loc} @ T_{loc}	34 meV	60 meV

Fitting parameters are listed in Table 2.1. These are very close to those found in the literature [60]. At lower temperatures, the optical emission is mainly due to transitions from localized states. In this region, it is observed that the transition energy is linearly reduced as the temperature is increased. After reaching the delocalization temperature (T_{loc}), if the temperature is increased, carriers are thermally activated, and the conduction band population is increased. If the delocalization temperature is exceeded, the optical emission observed is mainly due to transitions from the conduction band. As observed in the figure, the fitting of the data with Varshni model is quite satisfactory for temperatures higher than 100 K for both samples, where localization effects are almost negligible.

To make an estimation of the localization energy, we can study different parameters [45]. First of all, a comparison of the delocalization temperatures can be made. In Fig. 2.24 we can clearly observe how the delocalization temperature T_{loc} is lower for the low-ion density QW (${T_{\mathrm{loc}}}^{\mathrm{IM2}} = 77\,\mathrm{K}$) than for the other sample, with a higher ${T_{\mathrm{loc}}}^{\mathrm{NIM2}}$ of 100 K. Another estimation for the localization energy is the difference from localized states measured from the PL experiments and the simulated gap energy. At the lowest temperature from our experimental setup, 16 K, the localization energy is (${E_{\mathrm{loc}}}^{\mathrm{IM2}} = 10\,\mathrm{meV}$), again lower than the localization energy of the sample with higher ion density, ${E_{\mathrm{loc}}}^{\mathrm{NIM2}} = 18\,\mathrm{meV}$. If this energy is estimated at the delocalization energy, the difference is higher, as shown in Table 2.2.

Additionally, we can observe the FWHM of the PL emission of the same samples NIM2 and IM2 (Fig. 2.24, right). We see in this image how the maximum of the FWHM occurs at higher temperatures in the NIM2 sample. This is again consistent with a deeper localization energy in the case of the sample grown conventionally with no ion deflection.

We thus conclude that the observed localization energy from GaInNAs QWs is strongly dependent on the ion density present in the chamber during

growth. The higher ion density causes the deeper the localized states. This effect could also be due to the structural properties discussed in the previous subsection, since it is known that QW morphology plays a fundamental role on the localization energy [45].

2.7 Conclusions

In this chapter, our contributions to the characterization and understanding of nitrogen rf plasmas, and the effect of the ions on the optical properties of GaInNAs QWs grown by MBE have been presented.

A novel in situ plasma characterization method, consisting in the use of a Bayard–Alpert gauge as a modified Langmuir probe, has been proposed and demonstrated. We used this technique to perform a reliable characterization of the ignited plasma. This proposed setup can be used for the characterization of plasma parameters exactly at the sample position. Combining this method with other widely extended standard plasma characterization techniques (as for example the OED), optimum plasma parameters (Nitrogen flux, rf applied power) can be chosen for the growth of high-quality quantum wells.

Using the modified Langmuir probe method, the presence of plasma ions impinging onto the surface of the sample was detected. Since the presence of these ions during growth reduces the quality of the QWs, the application of external static magnetic fields was proposed to deflect the flux of ions flowing from the nitrogen source toward the growing surface, thus reducing the density of charged particles impinging onto the surface. With the modified Langmuir probe an effective reduction of the ion current at the position of the sample was measured, assessing the effectiveness of the deflection method.

The effects of the ion density impinging onto the sample during the growth of GaInNAs layers grown on GaAs (111)B and (100) were presented. The results for both orientations are similar: It was found that samples grown under a higher ion density showed poorer optical (reduced intensity and broader emission) and structural quality (compositional fluctuations, QW undulation), as shown by combined experiments of microscopy (AFM and TEM), and luminescence techniques (PL and CL).

We found that using the proposed magnetic deflection, the ion density is effectively reduced and the overall quality of the GaInNAs quantum wells is therefore strongly increased. Particularly, on GaAs (100) it was shown that the application of a deflecting magnetic field during the growth yielded a strong reduction of lateral compositional modulation of the GaInNAs quantum wells. Finally, we found from PL experiments that the samples grown with higher ion density showed a more pronounced and a deeper localization energy than the optimal samples grown under the magnetic deflection.

Acknowledgments. Based on the research carried out over several years, this work has been supported by several sources: Spanish Ministerio de Educación

y Ciencia, FPU grant program (first author); European Union, Project No. IST-2000-26478-GINA1.5; Comunidad Autónoma de Madrid; and by the Spanish Ministerio de Educación y Ciencia, projects CICYT TIC2001-4950-E and CICYT TIC2001-3849.

References

1. W. Li, M. Pessa, T. Ahlgren, J. Decker, Appl. Phys. Lett. **79**, 1094 (2001)
2. S.G. Spruytte, M.C. Larson, W. Wampler, C.W. Coldern, H.E. Petersen, J.S. Harris, J. Crys. Growth **227–228**, 506 (2001)
3. Z. Pan, L.H. Li, W. Zhang, Y.W. Lin, R.H. Wu, W. Ge, Appl. Phys. Lett. **77**, 1280 (2000)
4. J. Miguel-Sánchez, A. Guzmán, E. Muñoz, Appl. Phys. Lett. **85**, 1940 (2004)
5. J. Miguel-Sánchez, A. Guzmán, J.M. Ulloa, A. Hierro, E. Muñoz, J. Crys. Growth **278**, 234 (2005)
6. H. Carrère, A. Arnoult, A. Ricard, X. Marie, T.H. Amand, E. Bedel-Pereira, Sol. State Elect. **47**, 419 (2003)
7. H. Carrère, A. Arnoult, A. Ricard, E. Bedel-Pereira, J. Crys. Growth **243**, 295 (2002)
8. A. Grill, *Cold Plasma in Materials Fabrication: From Fundamentals to Applications* (Wiley-IEEE Press, New York 1994)
9. M.R. Wertheimer, M. Moisan, (1994) Pure and Appl. Chem. **66**, 1343
10. M. Kondow, K. Uomi, A. Niwa, T. Kitatani, S. Watahiki, Y. Yazawa, Jpn. J. Appl. Phys. Part 1 **35**, 1273 (1996)
11. I.A. Buyanova, W.M. Chen, B. Monemar, MRS Internet J. Nitride Semicond. Res. **6**, 2 (2001)
12. T. Kitatani, K. Nakahara, M. Kondow, K. Uomi, T. Tanaka, J. Cryst. Growth **209**, 345 (2000)
13. D.L. Smith, Solid. State. Commun. **57**, 919 (1986)
14. J.L. Sánchez-Rojas (1995) Contribución a la caracterización y aplicaciones de heteroestructuras piezoeléctricas de InGaAs, Doctoral Thesis, Universidad Politécnica de Madrid
15. J.M. Ulloa (2005) Diseño, fabricación y caracterización de diodos láser basados en pozos cuánticos de InGaAs(N)/GaAs', Doctoral Thesis, Universidad Politécnica de Madrid
16. J. Hernando (2002) Crecimiento por MBE, fabricación y caracterización de detectores de infrarrojos de pozo cuántico de InGaAs/GaAs, Doctoral Thesis, Universidad Politécnica de Madrid
17. J.J. Sánchez (2000) Crecimiento por MBE, fabricación y caracterización de láseres de AlGaAs/GaAs/InGaAs/GaAs (111)B para..., Doctoral Thesis, Universidad Politécnica de Madrid
18. I.W. Tao, W.I. Wang, Electron. Lett. **28**, 705 (1992)
19. A. Ishihara, H. Watanabe, Jpn. J. Appl. Phys. **33**, 1361 (1994)
20. T. Takeuchi, K. Muraki, Y. Hanamaki, S. Fukatsu, N. Yamada, N. Ogasawara, N. Mikoshiba, Y. Shiraki, J. Cryst. Growth **150**, 1338 (1995)
21. T. Fleischmann, M. Moran, M. Hopkinson, H. Meidia, G.J. Rees, J.L. Sanchez-Rojas, I. Izpura, J. Appl. Phys. **89**, 4689 (2001)

22. K.W. Goosen, E.A. Caridi, T.Y. Chang, J.B. Stark, D.A.B Miller, R.A. Morgan, Appl. Phys. Lett. **56**, 715 (1990)
23. E.A. Khoo, A.S. Pabla, J. Woodhead, J.P.R David, R. Grey, G.J. Rees IEE Proc.-Optoelectron. **145**, 62 (1999)
24. E.A. Khoo, J. Woodhead, J.P.R David, R. Grey, G.J. Rees Electron. Lett. **35**, 150 (1999)
25. V. Ortiz, N.T. Pelekanos, Appl. Phys. Lett. **77**, 788 (2000)
26. T. Fleischmann, J.M. Ulloa, M. Moran, G.J. Rees, J. Woodhead, M. Hopkinson, Microelectron. J. **33**, 547 (2002)
27. J. Miguel-Sánchez, A. Guzmán, J.M. Ulloa, A. Hierro, M. Montes, E. Muñoz, Photon. Technol. Lett. **17**, 2271 (2005)
28. T. Anan, K. Nishi, S. Sugou, Appl. Phys. Lett. **60**, 3159 (1992)
29. H.G. Colson, D.J. Dunstan, J. Appl. Phys. **81**, 2898 (1997)
30. S.P. Edirisinghe, A.E. Staton-Bevan, R. Grey, J. Appl. Phys. **82**, 4870 (1997)
31. M. Gutiérrez, D. González, G. Aragón, R. García, M. Hopkinson, J.J. Sánchez, I. Izpura, Appl. Phys. Lett. **80**, 1541 (2002)
32. H. Yamaguchi, M.R. Fahy, B.A. Joyce, Appl. Phys. Lett. **69**, 776 (1996)
33. M. Henini, S. Sanguinetti, L. Brusaferri, E. Grilli, M. Guzzi, M.D. Upward, P. Moriarty, P.H. Beton, Microelectron. J. **28**, 933 (1997)
34. F.Y. Tsai, C.P. Lee, J. Appl. Phys. **84**, 2624 (1997)
35. S. Sanguinetti, M. Gurioli, M. Henini, Microelectron J. **33**, 583 (2002)
36. P.P. González-Borrero, D.I. Lubyshev, E. Petitprez, N. La Scala Jr, E. Marega Jr., P. Basmaji, Brazilian J. Phys. **27**, 65 (1997)
37. W. Jiang, H. Xu, B. Xu, W. Zhou, Q. Gong, D. Ding, J. Liang, Z. Wang, J. Vac. Sci. Technol. B **19**, 197 (2001)
38. S.L. Tyan, P.A. Shields, R.J. Nicholas, F.Y. Tsai, C.P. Lee, Jpn. J. Appl. Phys. **39**, 3286 (2000)
39. F.Y. Tsai, C.P. Lee, Jpn. J. Appl. Phys. **38**, 558 (1999)
40. A.J. Ptak, K.S. Ziemer, M.R. Millecchia, C.D. Stinespring, T.H. Myers, MRS Internet J. Nitride Semicond. Res. **4S1**, G3.10 (1999)
41. M.A. Herman, H. Sitter, (1989) Molecular Beam Epitaxy: Fundamentals and Current Status, Springer, Berlin Heidelberg New York
42. J. Miguel-Sanchez, A. Guzman, J.M. Ulloa, A. Hierro, E. Muñoz IEE Proc. Optoelectron. **151**, 305 (2004)
43. J.M. Reifsnider, M.M. Oye, S. Govindaraju, A.L. Holmes Jr., J. Crys. Growth **280**, 7 (2005)
44. R.J. Molnar, T.D. Moustakas, J. Appl. Phys. **76**, 4587 (1994)
45. A. Hierro, J.M. Ulloa, J.M. Chauveau, A. Trampert, M.A. Pinault, E. Tournié, A. Guzmán, J.L. Sanchez-Rojas, E. Calleja, J. Appl. Phys. **94**, 2319 (2003)
46. K. Kim, A. Zunger, Phys. Rev. Lett. **86**, 2609 (2001)
47. S. Karirinne, E.M. Pavelescu, J. Kontinnen, T. Jouhti, M. Pessa New J. Phys. **6**, 192 (2004)
48. K. Uno, M. Yamada, I. Tanaka, O. Ohtsuki, T. Takizawa, J. Crys. Growth **278**, 214 (2005)
49. M. Kondow, T. Kitatani, S. Shirakata, J. Phys. Condens. Matter **16**, S3229 (2004)
50. E. Runge, J. Menniger, U. Jahn, R. Hey, H.T. Grahn, Phys. Rev. B **52**, 12207 (1995)
51. U. Jahn, O. Brandt, A. Trampert, P. Waltereit, R. Hey, K.H. Ploog, Mat. Sci. Eng. B, **91–92**, 329 (2002)

52. Y. Park, M.J. Cich, R. Zhao, P. Specht, H. Feick, E.R. Weber Phys. B: Condens. Matter, **308–310**, 98 (2001)
53. A. Trampert, J.M. Chauveau, K.H. Ploog, E. Tournié, A. Guzmán, J. Vac. Sci. Technol. B **22**, 2195 (2004)
54. H.F. Liu, S. Karirinne, C.S. Peng, T. Jouhti, J. Konttinen, M. Pessa, J. Cryst. Growth **263**, 171 (2004)
55. M.O. Fischer, M. Reinhardt, A. Forchel, IEEE J. Sel. Top. Quantum Electron. **7**, 149 (2001)
56. J.M. Chauveau, A. Trampert, K.H. Ploog, M.A. Pinault, E. Tournié, Appl. Phys. Lett. **82**, 3451 (2003)
57. J.M. Chauveau, A. Trampert, M.A. Pinault, E. Tournié, K. Du, K.H. Ploog, J. Crys. Growth **251**, 383 (2003)
58. M. Albrecht, V. Grillo, T. Remmele, H.P. Strunk, A.Y. Egorov, G.H. Dumitras, H. Riechert, A. Kaschner, R. Heitz, A. Hoffmann, Appl. Phys. Lett. **81**, 2719 (2002)
59. I.A. Buyanova, W.M. Chen, C.W. Tu, Semicond. Sci. Technol. **17**, 815 (2002)
60. M.A. Pinault, E. Tournié, Appl. Phys. Lett. **78**, 1562 (2001)

http://www.springer.com/978-3-540-74528-0

Dilute III-V Nitride Semiconductors and Material Systems
Physics and Technology
Erol, A. (Ed.)
2008, XXXII, 592 p., Hardcover
ISBN: 978-3-540-74528-0